Solution-State Conformational Ensemble of a Hexameric Porphyrin Array Characterized Using Molecular Dynamics and X-ray Scattering

Kristy L. Mardis,*,† Heather M. Sutton,† Xiaobing Zuo,§ Jonathan S. Lindsey,‡ and David M. Tiede*,§

Department of Chemistry and Physics, Chicago State University, Chicago, Illinois 60628, Department of Chemistry, North Carolina State University, Raleigh, North Carolina, 27695, and Chemistry Division, Argonne National Laboratory, Argonne, Illinois 60439

Received: September 18, 2008; Revised Manuscript Received: January 4, 2009

Solution-phase X-ray scattering measurements in combination with coordinate-based modeling have been used to characterize the conformational ensemble of a hexameric, diphenylethyne-linked porphyrin array in solution. Configurationally broadened X-ray scattering patterns measured at room temperature for dilute toluene solutions of the porphyrin array were compared to scattering patterns calculated from structural ensembles in constant pressure and temperature molecular dynamics simulations. Thermal fluctuations sampled at picosecond intervals within nanosecond time scale dynamic simulations show large-amplitude motions that include porphyrin ring "tipping" around the porphyrin linkage axes and extended hexameric porphyrin array "breathing" motions involving torsional distortions collectively distributed along porphyrin and diphenylethyne groups. Each type of group motion produced characteristic, angle-dependent dampening of scattering features that are needed to reproduce dampening features in the experimental X-ray scattering. However, mismatches in the magnitudes of experimental and simulated dampening of high-angle X-ray scattering patterns show that large-amplitude hexamer array breathing-type motions are significantly under-represented in the simulated ensembles. This comparison between experiment and simulation provides a means not only to interpret scattering data in terms of an explicit atomic model but more generally demonstrates the use of solution X-ray scattering as an experimental benchmark for the development of simulation methods that more accurately predict configurational dynamics of supramolecular assemblies.

Introduction

The development of chemistries that control the adaptive and dynamic features of supramolecular architectures beyond the molecular scale is central to the challenge of developing synthetic chemical approaches that embody biomimetic mechanistic principles.[1,2] Dynamic features of supramolecular architectures involve complex, nested atomic fluctuations across multiple length scales and a hierarchy of covalent and noncovalent interactions. Progress toward understanding the conformational dynamics of supramolecular architectures has been impeded by the lack of suitable tools for measuring and modeling conformational dynamics of supramolecular assemblies in solution and other noncrystalline media with atomic-scale precision.

Whereas spectroscopic measurements have been successful in providing site-selective markers for supramolecular conformation,[3−5] our most detailed understanding of the configurational landscapes populated by supramolecular assemblies in solution is primarily derived from molecular simulations. Molecular simulations are compelling because they provide an all-atom "molecular movie" of configuration dynamics based on fundamental physical principles, atomic force fields, and molecular mechanics. As such, they present a statement of our understanding of the fundamental principles that drive the chemistry. However, the accuracy of the molecular simulations for predicting functional properties of complex, nanoscale supramolecular architectures is limited both by the numerical challenges of applying first-principles computations to large molecular systems and by uncertainties in verifying the accuracies of simulations that necessarily utilize multiscale coarse-grained, continuum, and semiempirical methods.[6]

Recently, we have introduced the use of solution-phase X-ray scattering in combination with coordinate-based modeling as an experimental approach to achieving atomic-scale insight into the structure and conformational dynamics of supramolecular architectures in solution.[7−9] Solution-phase X-ray scattering provides a valuable and possibly unique all-atom measure of atomic pair distances, resolvable from single bond distances to the nanometer range, that are directly relatable to atomic structure by Fourier transform.[10−13] We have demonstrated the sensitivity of solution-phase scattering patterns to supramolecular conformation.[7−9,14,15] Furthermore, solution-state measurements necessarily include the pair−distance broadening due to configurational ensembles and hence provide an experimental marker of the ensemble that can be directly compared to atomistic molecular simulation.[7−9] The use of combined X-ray scattering and molecular modeling approaches allows the details of supramolecular dynamics to be developed at a fundamental, first-principles level using molecular simulations that are tested and evaluated for accuracy against X-ray scattering experiments.[8]

In the present work, we have tested the feasibility of combining X-ray scattering experiments and molecular dynamics simulations for the evaluation of supramolecular dynamics using the cyclic diphenylethyne-linked porphyrin hexamer shown in

---

* Corresponding authors. E-mail: kmardis@csu.edu, tiede@anl.gov.

† Chicago State University.

‡ North Carolina State University.

§ Argonne National Laboratory.

10.1021/jp808318x CCC: $40.75

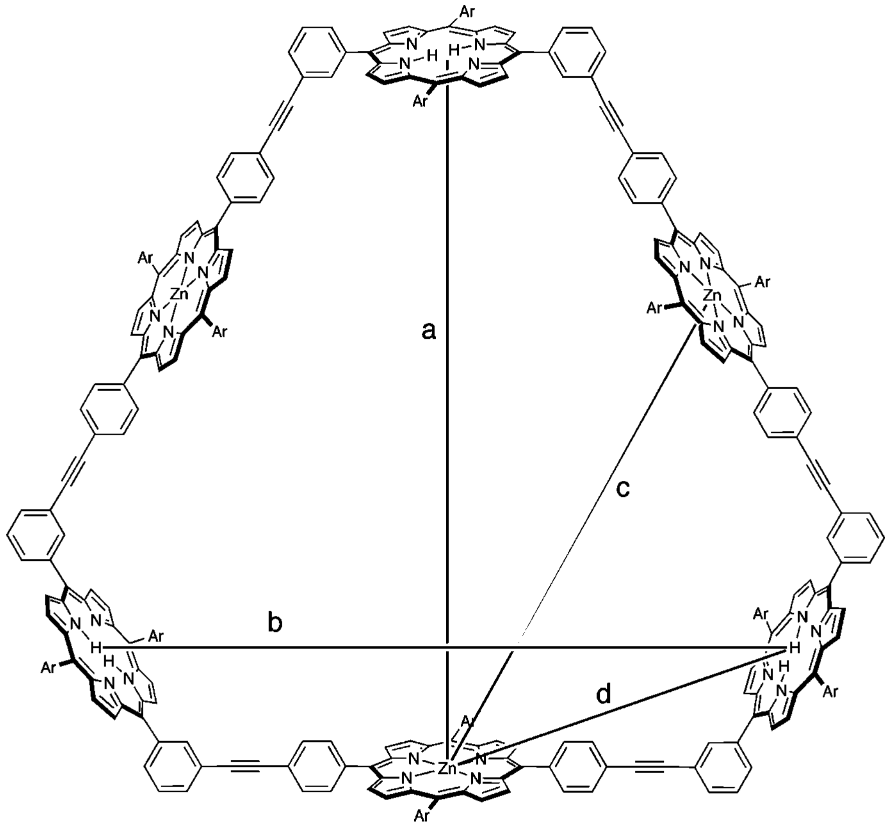

Figure 1. Structure of the diphenylethyne-linked porphyrin architecture, **1**, composed of a cyclic array of alternating zinc and free-base porphyrins (Ar = 2,4,6-trimethylphenyl). The porphyrin pair distances resolvable by solution-phase scattering measurements are labeled a−d.

Figure 1.[16] The cyclic porphyrin hexamer is an excellent test substrate for such studies for several reasons:

First, the array is a relatively large shape-persistent macrocycle with an ~35 Å diameter cavity.[16] Shape-persistent macrocycles are of interest for a variety of fundamental studies in materials science and serve as valuable architectures for biomimetic studies.[4,5,17]

Second, the array affords a variety of different molecular motions. The overall architecture incorporates six relatively modular rigid subunits (porphyrins) constrained in a macrocyclic ring via diphenylethyne linkers, yet the six porphyrins are divided into an alternating pattern of two types (zinc porphyrin and free base porphyrin) and are connected via p,p-substituted or m,p-substituted diphenylethyne linkers. Analogous arrays are available with a variety of patterns of metalation[18] and peripheral substitution.[19] Note that even with a uniform metalation state of the six porphyrins, the array (nominal 3-fold symmetry) is not a regular hexagon owing to the two types of substituted diphenylethyne linkers. As such, the hexamer array provides an architecture for testing our ability to detect and model nanoscale, supramolecular dynamics that are a composite of hierarchical local-site motions.

Finally, the array serves as a model for a covalently linked light-harvesting array[16] and as a host architecture for the assembly of a variety of light-harvesting arrays for solar energy conversion.[20−22] Self-assembly occurs upon metal coordination of chromophore guests whose ligand groups are designed to match synthetically varied positions of metallated porphyrins within the hexamer array.[21,22] Excited-state energy transfer occurs predominantly via a through-bond mechanism among covalently linked porphyrins in the array backbone and a through-space mechanism between such porphyrins and guest chromophores in the self-assembled host−guest complex.[21,22]

Prior X-ray scattering measurements for **1** found that scattering patterns are configurationally broadened and that the broadening could be reasonably fit using analytical models that included effects of porphyrin group rigid-body rotation and positional displacements.[7] However, the rigid-body analysis is an empirical approach for describing the solution-state ensemble and does not provide a coordinate model that can be fundamentally correlated with chemical function. This study investigates the feasibility of combining molecular dynamics simulations with X-ray scattering as a means to develop experimentally validated coordinate models for supramolecular solution-state ensembles. The development of accurate coordinate models for solution-state ensembles of light-harvesting materials is of significance for the understanding of self-assembling and repair properties, and for understanding the consequences of configuration dispersion on light-harvesting and solar energy conversion. Such an understanding is of particular relevance to more detailed insight into the dynamics of through-space energy transfer in self-assembled host−guest complexes derived from array **1**. Accurate models for solution-state structures may also be applicable for a wide variety of cyclic arrays.[23] More generally, experimental solution-phase X-ray-scattering-based modeling approaches will have applications for a broad range of macromolecular solution-state phenomena, including drug design[24] and catalysis.[25−28]

Method of Simulation. The initial structure for the hexameric, diphenylethyne-linked porphyrin cyclic array (Figure 1) was constructed using Hyperchem (Hypercube, Inc.). This structure was solvated in a cubic box with 55 Å sides containing 960 molecules of toluene to give a density to match the experimental conditions of liquid toluene. The toluene box was equilibrated ($E_{\text{fluc}}/\langle E \rangle < 10^{-5}$) before the box was used to solvate the porphyrin array.

Force field atom types and parameters were taken from the CHARMM 22 force field[29,30] with a few modifications. Whereas the standard porphyrin model contains iron, the current complex has three Zn(II) chelated porphyrin residues. The zinc parameters were taken from the work of Stote and Karplus.[31] These parameters assume only nonbonded interactions between the zinc and the surrounding porphyrin chelate. In addition, the porphyrins are connected by diphenylethyne linkers, each of which contains two triply bonded carbon linker atoms. Because CHARMM 22 does not have parameters for triple-bonded carbons, bond distances and the CA−C#−C#−CA dihedral parameters were developed using standard methods. A dihedral value for k_θ of 0.38 kcal/mol/deg was determined by fitting the torsional barrier calculated at the Hartree−Fock 6-31G* level for a 1-methyl-3-(phenylethynyl)benzene test system to the CHARMM dihedral energy function. The partial atomic charges (available in Supporting Information) were taken from the protoporphyrin IX structure in the Quanta 98 implementation of CHARMM 22. The aromatic ring charges were chosen to match those of aromatic rings and aliphatic groups in CHARMM 22.

The molecular dynamics simulations were performed for 2.05 ns (time step was 1 fs) at room temperature using the program CHARMM.[32] Standard periodic boundary conditions were employed with atom-based cutoffs of 13 Å using a force shift.[33] The system was initially heated for 10 ps and then the Hoover constant-pressure thermostat was used for the equilibration (340 ps). During the production time period, coordinates were saved every 1 ps for later analysis. Two additional, identical runs with new random seeds were carried out to check the reproducibility of results. Furthermore, an additional 0.75 ns of simulation time was performed for one of the runs to determine if longer simulation times affected the results.

At the conclusion of the simulation, the orientationally averaged scattering profile, $I(q)$, was calculated for each set of coordinates (**r**) using eq 1[8,12,34]

$$I(q) = \sum_{j}^{N} \sum_{k}^{N} A_j A_k \frac{\sin(qr_{j,k})}{qr_{j,k}} \tag{1}$$

The atomic scattering amplitudes are of the form

$$A_j = f_j(q) e^{-B_j q^2/16\pi^2} - g_j(q) \tag{2}$$

The atomic X-ray scattering form factors, $f_j(q)$,[35] and the atomic excluded solvent form factors, $g_j(q)$,[12] were taken from the literature and are available in Supporting Information. The individual scattering functions were then averaged over all snapshots for comparison to the experimental scattering data.

Results and Discussion

Comparing the X-ray Scattering Experiment and Simulation. A comparison of the X-ray scattering experiment with simulated scattering patterns calculated from two coordinate models is shown in Figure 2. The first model was that of a single energy-minimized structure, and the second model was taken from an ensemble of 1700 conformers obtained during a 2.05 ns constant pressure MD simulation of the hexameric porphyrin array in toluene. Scattering from the ensemble was calculated as the average of the individual scattering patterns from each of the 1700 conformers. The energy-minimized structure provides a single structure that might be expected to be representative of the solution ensemble, whereas scattering calculated from the entire MD ensemble tests the ability of the MD ensemble to represent the actual solution-state conformational dispersion measured by experiment. The scattering patterns are plotted with arbitrary vertical scaling as a function of the magnitude of the scattering vector, q, which is related to the scattering angle 2θ by the relation $q = (4\pi/\lambda) \sin \theta$, where λ is the X-ray wavelength. The experimental scattering was taken from work reported previously.[7]

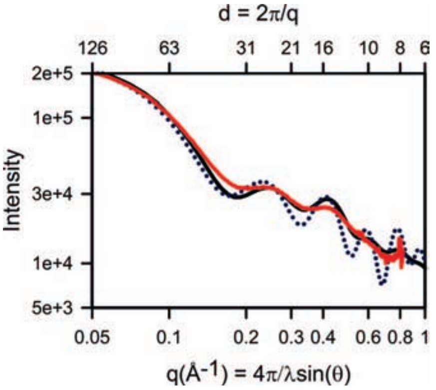

Figure 2. Experimental and calculated scattering patterns for porphyrin hexamer **1**. Experimental data (red) are compared with the calculated scattering pattern for an energy-minimized structure (dotted) and the MD ensemble average (black).

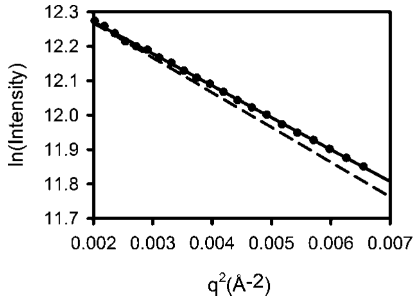

Figure 3. Guinier plots for the experimental scattering data (●), the scattering calculated from an energy-minimized structure (---), and the MD ensemble scattering (−) calculated as the average of the scattering from all conformers.

A measure of the overall size of the supramolecular array is provided by fitting the scattering in the small-angle region defined by the condition $q < 1/R_g$, where R_g is the radius of gyration, using the Guinier relationship

$$I(q) = \ln[I(0)] - \frac{q^2 {R_g}^2}{3} \tag{3}$$

with $I(0)$ defined as the forward-scattering amplitude.[36,37] Experimental scattering data and scattering calculated from the energy-minimized and MD models are all seen to follow a linear relationship in the region of $q < 0.1$ Å^{-1} as shown by the plots in Figure 3. The experimental scattering and MD ensemble model scattering are close to indistinguishable, and slopes of the lines correspond to R_g values of 16.8 (±0.1) Å for the experiment and 16.7 (±0.2) Å for the MD ensemble averaged over three simulation runs. In contrast, the scattering for the energy-minimized structure deviates from experimental scattering and has an R_g value of 17.1 Å, reflecting a structure that is larger than those found in the experimental and MD ensemble averages.

Scattering in the $0.1 \text{ Å}^{-1} < q < 1.0 \text{ Å}^{-1}$ region interrogates structure across the 60 to 6 Å spatial resolution range ($d = 2\pi/q$). This scattering region provides the most direct measure of the hexameric ring conformation. In this region, scattering for the hexameric cyclic porphyrin array is characterized by oscillatory interference that can be shown by indirect inverse Fourier transform of the scattering within the experimental q range to produce a pair distance distribution function (PDDF) that resolves into a set of peaks associated with the four sets of porphyrin pairs indicated in Figure 1.[7] For the cyclic hexameric architecture, the porphyrin **a** and **b** pairs have overlapping atom pair distances, and in the PDDF, these distances are merged within a single peak whereas the pair correlations for the **c** and **d** porphyrin pairs are resolved as separate peaks.[7] The position of the **a** + **b** PDDF peak is a measure of the overall dimensions of the supramolecular ring. Both scattering and corresponding PDDF patterns provide sensitive markers of the hexameric porphyrin array conformation.

A comparison of the experimental and model scattering patterns in the $0.1 \text{ Å}^{-1} < q < 1.0 \text{ Å}^{-1}$ region in Figure 2 shows that the energy-minimized structure only approximately reproduces the oscillatory peak positions seen in experiment and dramatically deviates from experiment in the amplitude of the oscillatory pattern. The difference in the oscillatory peak pattern has been shown to correspond to a 1.4 Å compression of the overall dimension of the hexameric ring measured in experiment compared to the energy-minimized structure, and the stronger oscillatory pattern can be understood to reflect the prominent interference from a static, single conformer structure.[7] In contrast, the scattering pattern calculated from the MD ensemble is found to provide a better model for the experimental scattering data, notably by close matching of the position of the first oscillatory peak and by the strong dampening of oscillatory features, particularly in the q range above 0.5 Å^{-1}. The alignment of the first oscillatory scattering peak can be seen to correspond to an agreement in the overall dimensions of the hexameric array, as shown by the matching of the porphyrin pair **a** + **b** PDDF peaks (Figure S1, Supporting Information). A summary of PDDF parameters derived from the models and experiment is presented in Table S1. Model-dependent changes in the overall dimension of the hexameric array are also reflected in the R_g measurements described above.

The most obvious difference between the scattering calculated from the MD ensemble and experiment is the insufficient dampening of the first two oscillatory peaks in the $0.2 \text{ Å}^{-1} < q < 0.5 \text{ Å}^{-1}$ region calculated from the MD ensemble. The additional dampening seen in the experiment is indicative of structural fluctuations on a length scale comparable to the dimensions of the hexameric array. To gain insight into the kinds of molecular motions that can be expected to contribute to this type of experimental broadening, we examined correlations between structures for individual conformers within the MD ensemble and the corresponding calculated scattering features, as described below.

Solution-State Ensembles in Simulation and Experiment. Distance-dependent structural fluctuations are an inherent feature of thermal fluctuations for a supramolecular array and are directly detected in an X-ray scattering experiment by q-dependent broadening of X-ray scattering features. Figure 4 shows the scattering patterns for each of the 1700 conformers within the MD simulation plotted along with the average of these patterns and the experimental data. In this plot, the scattering for each conformer is plotted as a gray line, and the ensemble forms a shaded area that is the reciprocal space representation of distance-dependent atomic pair disorder simulated in solution. The simulation shows a root-mean-square deviation of atomic positions in the ensemble of 3.8 Å.

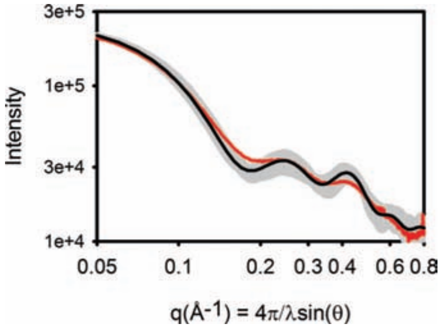

Figure 4. X-ray scattering calculated for a solution-state conformation ensemble for the cyclic porphyrin hexamer produced by MD simulation. Scattering patterns were calculated for individual snapshots taken every 1 ps during the production phase of the simulation and are plotted in gray. The average of all scattering patterns in the ensemble is shown in black, and the experimental data are shown in red.

A comparison of the q-dependent dampening of scattering features in MD simulation to experiment in Figure 4 shows that ensemble broadening provides a mechanism to account for dampening in the q region above 0.5 Å^{-1} but not in the $0.1 \text{ Å}^{-1} < q < 0.5 \text{ Å}^{-1}$ region. This finding suggests that the simulated ensemble fails to provide a model that adequately accounts for long-range structural disorder that is present in experiment. Various large-amplitude thermal fluctuations are observed within the dynamic simulations, predominantly including porphyrin ring "tipping" around the porphyrin linkage axes and extended hexameric array "breathing" motions involving torsional distortions collectively distributed along porphyrin and diphenylethyne groups. Each type of group motion is found to produce characteristic, angle-dependent dampening of scattering features. These large-amplitude group motions are significant because they provide models for long-range atomic disorder that underlies q-dependent dampening of X-ray scattering observed in experiment.

Hexameric Array Breathing Motions. The amplitude and position of the first oscillatory peak in scattering patterns for a ringlike structure is a function of both the dimensions and symmetry of the ring. To track these properties for each of the conformers in the MD simulation, we introduced a conformation index for the hexameric array defined by the area of a triangle formed by connecting the three zinc atoms. A linear correlation was found between this area index and the amplitude of the first scattering peak as shown by the plot in Figure 5. The average value of the area index in the MD ensemble is 279 Å^2 (σ=24 Å^2), which can be compared to a value of 262 Å^2 for the energy-minimized starting structure. The correspondence between this area index and molecular conformation is illustrated in Figure 6, showing representative conformers with area indices taken near the average (280 Å^2), maximum (342.5 Å^2), and minimum (198.3 Å^2) values in the distribution. The scattering patterns corresponding to these conformers are shown in Figure 7. The maximum value can be seen to be associated with a bowing distortion along the Zn-porphyrin sides, producing an expanded hexameric array structure. In the scattering pattern, this feature is correlated with a significant enhancement in the amplitude of the first interference peak and shifts to lower q reflecting the longer atom pair correlations. Conversely, the conformer with the minimum area marker is seen to be associated with distortions in the diphenylethyne linkers that allow one or more of the porphyrin groups to rotate along an

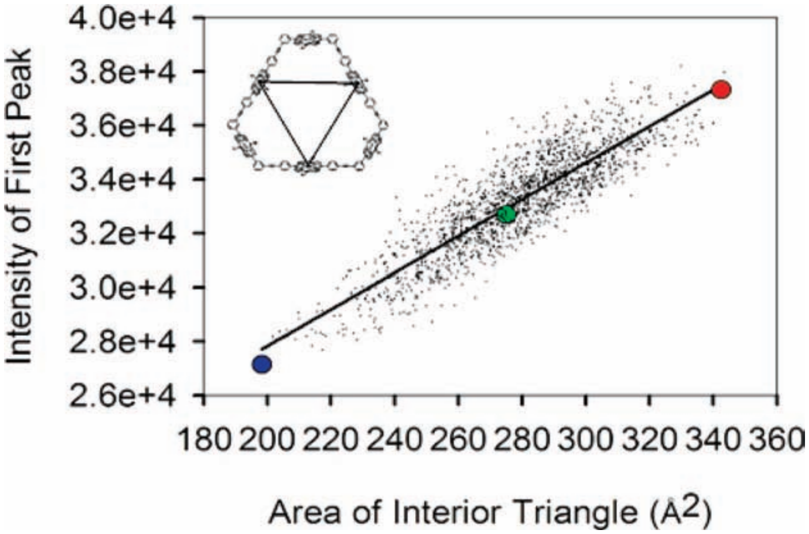

Figure 5. Correlation between the height of the peak at $q = 0.2$ Å^{-1} and the area of the triangle with the three zinc atoms at the vertices. $R^2 = 0.79$. Each point represents a time snapshot with the points highlighted in color corresponding to the structures shown. For reference, the energy-minimized highly organized starting structure has an area of 262 Å^2.

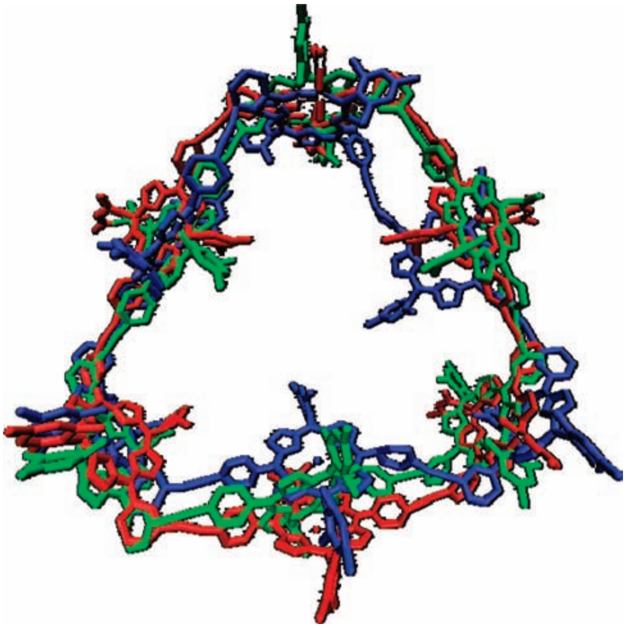

Figure 6. Porphyrin array structures representative of conformers that have area index values near the maximum (red), minimum (blue), and average (green) found in the MD ensemble. The positions of these conformers within the ensemble are shown by colored dots in Figures 5 and 8. The area index values for these structures are 342.5, 198.3, and 275.2 Å^2, respectively.

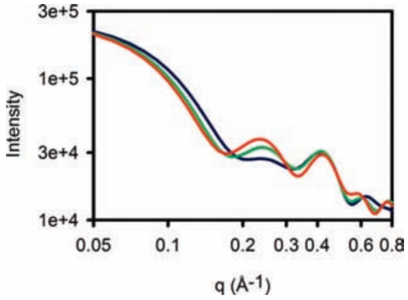

Figure 7. Calculated scattering profiles for porphyrin array structures representative of conformers with area index values near the maximum (red), minimum (blue), and average (green) found in the MD ensemble. The positions of these conformers within the ensemble are shown by colored dots in Figures 5 and 8. The structures for these conformers are shown in Figure 6 with the area indices listed in the figure legend and discussed in the text.

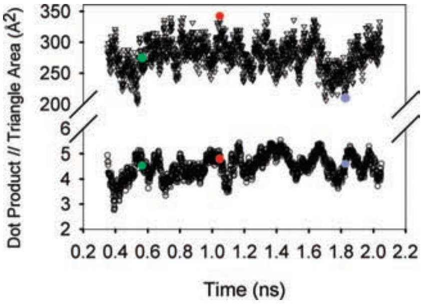

Figure 8. Porphyrin hexamer array conformation area index (▽) and porphyrin tipping index, T_t (○), plotted for each snapshot during the production phase of the simulation. The points from Figure 5 are highlighted in the same color scheme as in Figures 5−7 for reference.

axis perpendicular to the plane of the hexameric array and produces a significant asymmetric distortion. The scattering pattern shows a corresponding attenuation of the first interference peak and a slight shift to higher q. Comparison to the experimental data suggests that these highly distorted conformers are more significantly populated in the experimental ensemble than in the simulated one. An increase in the population of the highly distorted conformers in the simulated ensemble would bring the simulated and experimental scattering patterns into better alignment with respect to both the amplitude of the first interference peak and the slope of the scattering in the 0.1−0.2 Å^{-1} q region.

A plot of the array breathing motion marker as a function of time (Figure 8) shows a combination of rapid transition spikes lasting 20 ps or less as well as motions that result in local minima lasting for as long as 0.2 ns. The downward spikes typically appear to involve single porphyrin group rotation perpendicular to the hexamer array, and the upward spikes are associated with the array doming motions as described above. The longer-lifetime transitions tended to involve multiple group motions. Similar results for additional simulation runs are shown in Figures S2 and S3 in the Supporting Information.

Porphyrin Tipping Motions. In addition to the array breathing motions parametrized by the change in the area of the interior

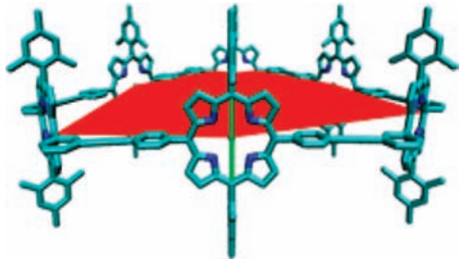

Figure 9. Structure of the hexameric array after initial energy minimization. The plane of the array is shown in red. An example of the vectors used to quantify the tilts of the porphyrin rings is shown by the green line drawn on the closest face-on porphyrin.

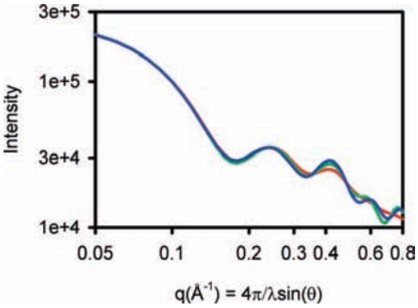

Figure 10. Effect of free base ring tipping on X-ray scattering. Three scattering patterns are calculated from conformers with T_{fb} values of 1.39 (red), 2.04 (green), and 2.30 (blue), and all had a hexameric array area index of approximately 300 Å^2.

triangle, the simulation structures also demonstrate considerable tipping of the porphyrin rings. When the hexameric array is built and energy-minimized using the CHARMM force field, the resultant structure is highly organized (Figure 9) with all porphyrin rings perpendicular to the plane of the hexamer array (shown in red). However, during the course of the simulation, the rings rotate with an average of two of the porphyrin rings being significantly tilted with respect to the plane of the structure at any given time. To quantify this tipping, vectors running parallel to the plane of each porphyrin ring were calculated (an example is shown as a green line in Figure 9), and the dot product between this vector in the snapshot and the same vector in the original, highly organized structure was obtained for all six porphyrin rings and summed (total tipping index, T_t). When all porphyrin rings are upright and perpendicular to the plane of the supramolecular structure, as they are in the energy-minimized structure, the sum of all dot products is 6. If one porphyrin ring is completely tipped into the plane of the complex, then a value of 5 is obtained. If two are tipped, the dot product is 4, and so forth. Likewise, tipping indices for the zinc (T_z) and free base (T_{fb}) porphyrin subsets were examined.

As shown in Figure 8, the rings are very mobile with the value of T_t fluctuating in time from a low of 2.76 to a high of 5.54. The simulation average is 4.5 ($\sigma = 0.4$). The porphyrin tipping motions produce significant modulation of all oscillatory scattering features. For conformer area indices greater than 298 Å^2, the ring tipping index of the free base subset strongly modulates the amplitude of the scattering peak at 0.4 $^{-1}$ in a predictable manner. Figure 10 compares scattering patterns for conformations that have a constant area index but vary in T_{fb}. For structures with larger than average area indices, increased tipping results in dampening of the scattering peak at 0.4 Å^{-1}. This pattern is less clear for conformers with smaller area indices or as a function of the total porphyrin tipping index because the tipping of the zinc porphyrins and the conformers with low area indices tend to be associated with deformations that decrease the symmetry of the hexameric array. Whereas both hexameric array breathing and individual porphyrin ring tipping motions are found to provide a mechanism for the dampening of X-ray scattering oscillatory patterns, the incomplete dampening of these scattering features in the simulated ensemble suggests that these motions are under-represented in the simulated ensemble compared to that observed experimentally.

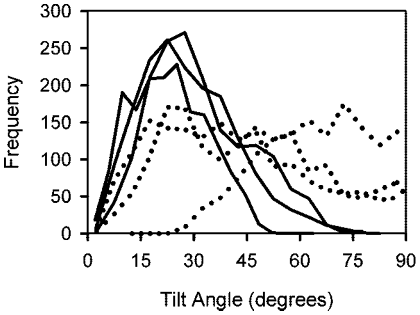

Figure 11. Histogram of the tilt angle in degrees for each of the six porphyrin rings. The histograms for the zinc porphyrins and free base porphyrins are represented by dotted and solid line traces, respectively. A tilt angle of 0° indicates that the porphyrin ring is perpendicular to the plane of the hexameric array.

Finally, it is interesting that the MD simulations show position-dependent variation in porphyrin ring tipping motions within the hexamer array architecture. In particular, the zinc porphyrins are seen to rotate to a greater degree than the free base porphyrins in the "corners" of the hexameric array. This can be seen by a plot of the histogram of the porphyrin tilt angle in the MD ensemble, shown in Figure 11. The three zinc porphyrins have a higher population of angles greater than 60° than do the free base porphyrins. The greater rotation of the zinc porphyrins versus the free base porphyrins does not stem from the metalation state of the porphyrin but rather from the different linker attached to the zinc versus free base porphyrins. The zinc porphyrin bears two *p*,*p*-diphenylethyne-substituted linkers and hence can rotate about the cylindrically symmetric ethyne bond as well as the single bond between the porphyrin meso carbon and the phenyl moiety. By contrast, the free base porphyrin bears two *m,p*-diphenylethyne-substituted linkers and hence can rotate only about the single bond between the porphyrin meso-carbon and the phenyl moiety.

Interestingly, each of the six porphyrins in the hexamer array has a distinguishable tipping histogram. For example, in comparing the histograms for the three zinc porphyrins shown in Figure 11, one is seen to have a smaller population of low tilt angles compared to the other two. Similarly, one of the free base porphyrins has a narrower tilt angle distribution than the other two. Repeating the simulation with different starting velocities results in similar patterns, but with the "outlying" histogram shifting to a different porphyrin in the group. Because the supramolecular array has 3-fold symmetry, this indicates that the simulation creates small inhomogeneities that remain for the length of the simulation. Longer simulations should result in a convergence of tilting behavior for porphyrins with equivalent linkers.

Implications for Simulation Development. Overall, thermal-driven conformational fluctuations in MD simulations were found to provide a mechanism that accounts for the dampening of high-angle scattering data but failed to account for the dampening of interference features at lower angles. In particular, the MD simulations were found to provide an insufficient population of conformers with distorted hexameric array geometries that are necessary to account for dampening the scattering peak observed at $q \approx 0.22$ Å^{-1} and also have an insufficient population of conformers with a high porphyrin tipping index to account for additional dampening of the scattering peak at $q = 0.44$ Å^{-1}. Raising the temperature of the simulations was found to improve only partially the agreement between simulation and experiment. For example, a simulation at 360 K resulted in a modest increase in the dampening of the scattering peak at $q = 0.44$ Å^{-1}, as shown in Figure S4. This supports the contention that the simulation ensemble requires structures with more flexibility in order to reproduce the experiment more accurately but that simulations within the 2 ns − 10 ns time frame at elevated temperature cannot fully reproduce the ensemble measured by the experiment. These shortfalls suggest that the force field parameters may be unrealistically stiff or that accessible time scales for simulation do not allow the full conformational landscape to be explored. Accelerated molecular dynamics[40−42] and multiscale methods[6] have been developed to provide more accurate simulation methods for modeling complex supramolecular dynamic landscapes. The scattering analysis described here provides a means to evaluate the ability of these advanced simulation methods to model solution-phase ensembles accurately compared to other experimental benchmarks that focus on a single, low-energy structure.

Correlation to the Energy-Transfer Function. The X-ray scattering with MD simulation analysis shows that the experimental solution-state ensemble is characterized by a significant population of conformations with distortions that lower the symmetry of the hexameric porphyrin array structure. These distortions produce conformers that have on average one or two porphyrins significantly displaced from their positions in a symmetric, energy-minimized structure. Despite the inequivalence in geometry between different porphyrin pairs resulting from the distortions within the hexamer array, nearest-neighbor zinc porphyrin to free base porphyrin excited-state energy transfer within the hexameric array architecture has been shown to follow homogeneous single-exponential kinetics with a 40 ps time constant,[22] suggesting that the through-bond energy transfer across the diphenylethyne linker is not noticeably dependent on the porphyrin and linker conformations. This conformation-independent energy-transfer behavior can be contrasted with conformation-dependent dispersion in electronic coupling observed between porphyrins connected through conjugated linkers[43,44] and in the electron transfer between donor and acceptor molecules connected through longer “molecular wire” linkers.[45,46]

Conclusions

Molecular dynamics simulations using the CHARMM 22 force field were used to provide an explicit atomic model for solution-state X-ray scattering for a porphyrin hexamer array. General features of the experimental X-ray scattering, including the overall shape, peak positions, and q-dependent dampening of oscillatory features were reproduced by the MD ensemble. These results indicate that the array undergoes extended breathing distortions and porphyrin tipping motions that induce conformational disorder. In fact, specific regions of variance between simulation and experiment were found to arise from the under-representation of long-range conformational disorder in the simulated ensemble. In particular, comparisons between the MD ensemble and experiment suggest that the simulation unrealistically restricts large-scale motions in the hexameric array. This work demonstrates the feasibility of using a combined simulation and X-ray scattering analysis to develop more accurate atomistic models of supramolecular solution-state conformational landscapes. The identified limits of the MD simulations will be incorporated into future analysis of the wide-angle ($q > 1$ Å^{-1}) region that contains structural information on solute−solvent interactions. Developing atomic-scale models of ensembles that include these interactions is critical to our ongoing work on the description of real-time structural dynamics of photoinitiated processes in supramolecular architectures.

Acknowledgment. This work was supported by the National Science Foundation IL-LSAMP grant HRD-0413000 (H.M.S. and K.L.M.), NIH-MBRS grant R25GM59218 (H.M.S.), and the Office of Science, Basic Energy Sciences, U.S. Department of Energy, under contract numbers DE-AC02-06CH11357 (D.M.T. and work at APS sector 12) and DE-FG02-96ER14632 (J.S.L.). K.L.M. thanks Dr. Sam Bowen for helpful discussions. We also acknowledge Dr. S. Seifert for his generous help and advice on synchrotron X-ray experiments.

Supporting Information Available: Atomic X-ray scattering form factors and volume factors used to calculate the atomic excluded solvent form factors. PDDF plots determined from experimental and model scattering. Porphyrin array conformation area index plots for two other simulation runs. Calculated scattering patterns for four other simulation runs. CHARMM rtf and par files for a porphyrin macrocycle. This material is available free of charge via the Internet at http://pubs.acs.org.

References and Notes

(1) Badjić, J. D.; Nelson, A.; Cantrill, S. J.; Turnbull, W. B.; Stoddart, J. F. *Acc. Chem. Res.* **2005**, *38*, 723–732.

(2) Lehn, J.-M. *Chem. Soc. Rev.* **2007**, *36*, 151–160.

(3) Grave, C.; Lentz, D.; Schäfer, A.; Samori, P.; Rabe, J. P.; Franke, P.; Schlüter, A. D. *J. Am. Chem. Soc.* **2003**, *125*, 6907–6918.

(4) Grave, C.; Schlüter, A. D. *Eur. J. Org. Chem.* **2002**, *307*, 5–3098.

(5) Moore, J. S. *Acc. Chem. Res.* **1997**, *30*, 402–413.

(6) Schatz, G. C. *Proc. Natl. Acad. Sci. U.S.A.* **2007**, *104*, 6885–6892.

(7) Tiede, D. M.; Zhang, R.; Chen, L. X.; Yu, L.; Lindsey, J. S. *J. Am. Chem. Soc.* **2004**, *126*, 14054–14062.

(8) Zuo, X.; Cui, G.; Mertz, K. M.; Zhang, L.; Lewis, F. D.; Tiede, D. M. *Proc. Natl. Acad. Sci. U.S.A.* **2006**, *103*, 3534–3539.

(9) O'Donnell, J. L.; Zuo, X.; Goshe, A. J.; Sarkisov, L.; Snurr, R. Q.; Hupp, J. T.; Tiede, D. M. *J. Am. Chem. Soc.* **2007**, *129*, 1578–1585.

(10) Vaughan, P. A.; Sturdivant, J. H.; Pauling, L. *J. Am. Chem. Soc.* **1950**, *72*, 5477–5486.

(11) Warren, B. E. *X-Ray Diffraction*; Dover Publications: New York, 1990; p 381.

(12) Svergun, D.; Barberato, C.; Koch, M. H. J. *J. Appl. Crystallogr.* **1995**, *28*, 768–773.

(13) Zhang, R.; Marone, P. A.; Thiyagarajan, P.; Tiede, D. M. *Langmuir* **1999**, *22*, 7510–7519.

(14) Tiede, D. M.; Zhang, R.; Seifert, S. *Biochemistry* **2002**, *41*, 6605–6614.

(15) Zuo, X.; Tiede, D. M. *J. Am. Chem. Soc.* **2005**, *127*, 16–17.

(16) Li, J.; Ambroise, A.; Yang, S. I.; Diers, J. R.; Seth, J.; Wack, C. R.; Bocian, D. F.; Holten, D.; Lindsey, J. S. *J. Am. Chem. Soc.* **1999**, *121*, 8927–8940.

(17) Höger, S. *J. Polym. Sci., Part A: Polym. Chem.* **1999**, *37*, 2685–2698.

(18) Yu, L.; Lindsey, J. S. *J. Org. Chem.* **2001**, *66*, 7402–7419.

(19) Tomizaki, K.-Y.; Yu, L.; Wei, L.; Bocian, D. F.; Lindsey, J. S. *J. Org. Chem.* **2003**, *68*, 8199–8207.

(20) Li, J.; Yu, L.; Lindsey, J. S. *Org. Lett.* **2000**, *2*, 2563–2566.

(21) Song, H.-E.; Kirmaier, C.; Schwartz, J. K.; Hindin, E.; Yu, L.; Bocian, D. F.; Lindsey, J. S.; Holten, D. *J. Phys. Chem. B* **2006**, *110*, 19121–19130.

(22) Song, H.-E.; Kirmaier, C.; Schwartz, J. K.; Hindin, E.; Yu, L.; Bocian, D. F.; Lindsey, J. S.; Holten, D. *J. Phys. Chem. B* **2006**, *110*, 19131–19139.

(23) Harvey, P. D. In *The Porphyrin Handbook*; Kadish, K. M., Smith, K. M., Guilard, R., Eds.; Academic Press: San Diego, CA, 2003; Vol. 18, pp 63−250.

(24) Teague, S. J. *Nat. Rev. Drug Discovery* **2003**, *2*, 527–541.

(25) Gianneschi, N. C.; Bertin, P. A.; Nguyen, S. T.; Mirkin, C. A.; Zakharov, L. N.; Rheingold, A. L. *J. Am. Chem. Soc.* **2003**, *125*, 10508–10509.

(26) Martinez, A. G.; Vilar, E. T.; Fraile, A. G.; de la Moya Cerero, S.; Martinez Ruiz, P.; Diaz Morillo, C. *Tetrahedron: Asymmetry* **2007**, *18*, 742–749.

(27) Fenimore, P. W.; Frauenfelder, H.; McMahon, B. H.; Young, R. D. *Proc. Natl. Acad. Sci. U.S.A.* **2004**, *101*, 14408–14413.

(28) Henzler-Wildman, K. A.; Lei, M.; Thai, V.; Kerns, S. J.; Karplus, M.; Kern, D. *Nature* **2007**, *450*, 913–919.

(29) MacKerell, A. D. J.; Wiorkiewicz-Kuczera, J.; Karplus, M. *J. Am. Chem. Soc.* **1995**, *117*, 11946–11975.

(30) MacKerell, A. D. J.; Bashford, D.; Bellott, M.; Dunbrack, R. L.; Evanseck, J. D.; Field, M. J.; Fischer, S.; Gao, J.; Guo, H.; Ha, S.; Joseph-McCarthy, D.; Kuchnir, L.; Kuczera, K.; Lau, F. T. K.; Mattos, C.; Michnick, S.; Ngo, T.; Nguyen, D. T.; Prodhom, B.; Reiher, W. E. I.; Roux, B.; Schlenkrich, M.; Smith, J. C.; Stote, R.; Straub, J.; Watanabe, M.; Wiorkiewicz-Kuczera, J.; Yin, D.; Karplus, M. *J. Phys. Chem. B* **1998**, *102*, 3586–3616.

(31) Stote, R. H.; Dejaegere, A.; Karplus, M. In *Computational Approaches to Biochemical Reactivity*; Náray-Szabó, G., Warshel, A., Eds.; Springer: New York, 1997; Vol. 19, pp 153−198.

(32) Brooks, B. R.; Bruccoleri, R. E.; Olafson, B. D.; States, D. J.; Swaminathan, S.; Karplus, M. *J. Comput. Chem.* **1983**, *4*, 187–217.

(33) Steinbach, P. J.; Brooks, B. R. *J. Comput. Chem.* **1994**, *15*, 667–683.

(34) Zhang, R.; Thiyagarajan, P.; Tiede, D. M. *J. Appl. Crystallogr.* **2000**, *33*, 565–568.

(35) Ibers, J. A.; Hamilton, W. C. *International Tables for X-ray Crystallography*; Kynoch Press: Birmingham, England, 1973; Vol. IV, pp 70−100.

(36) Guinier, A.; Fournet, G. *Small Angle Scattering of X-rays*; Wiley: New York, 1955; p 268.

(37) Cotton, J. P. In *Neutron, X-ray and Light Scattering*; Lindner, P., Zemb, T., Eds.; Elsevier Science Publishers B.V.: Amsterdam, 1991; pp 3−18.

(38) Lee, S. J.; Mulfort, K. L.; Zuo, X.; Goshe, A. J.; Wesson, P. J.; Nguyen, S. T.; Hupp, J. T.; Tiede, D. M. J. Am. Chem. Soc. 2008, in press.

(39) Lee, S. J.; Mulfort, K. L.; O'Donnell, J. L.; Zuo, X.; Goshe, A. J.; Nguyen, S. T.; Hupp, J. T.; Tiede, D. M. *Chem. Commun.* **2006**, 4581–4583.

(40) Donald, H.; John, M.; McCammon, J. A. *J. Chem. Phys.* **2004**, *120*, 11919–11929.

(41) Markwick, P. R. L.; Bouvignies, G.; Blackledge, M. *J. Am. Chem. Soc.* **2007**, *129*, 4724–4730.

(42) Yang, L. J.; Grubb, M. P.; Gao, Y. Q. *J. Chem. Phys.* **2007**, *126*, 125102. .

(43) Ahn, T. K.; Yoon, Z. S.; Hwang, I.-W.; Lim, J. K.; Rhee, H.; Joo, T.; Sim, E.; Kim, S. K.; Aratani, N.; Osuka, A.; Kim, D. *J. Phys. Chem. B* **2005**, *109*, 11223–11230.

(44) Winters, M. U.; Kärnbratt, J.; Blades, H. E.; Wilson, C. J.; Frampton, M. J.; Anderson, H. L.; Albinsson, B. *Chem.−Eur. J.* **2007**, *13*, 7385–7394.

(45) Davis, W. B.; Ratner, M. A.; Wasielewski, M. R. *J. Am. Chem. Soc.* **2001**, *123*, 7877–7886.

(46) Daub, J.; Engel, R.; Kurzawa, J.; Miller, S. E.; Schneider, S.; Stockmann, A.; Wasielewski, M. R. *J. Phys. Chem. A* **2001**, *105*, 5655–5665.

JP808318X